RSC Advances

ROYAL SOCIETY OF CHEMISTRY

www.rsc.org/advances

One-step synthesis of high-quality N-doped grapheme/Fe_3O_4 hybrid nanocomposite and its improved supercapacitor performances

Li Li, Yuanyun Dou, Lifeng Wang, Min Luo and Jun Liang*

College of Chemistry and Chemical Engineering, Ningxia University, Yinchuan 750021, P. R. China

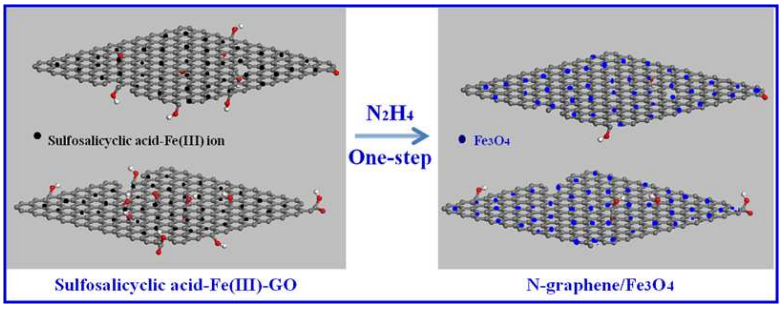

$$\left[Fe^{III}\left(\text{sulfosalicyclic acid}\right)_3\right]^{6-} + \text{Graphene oxide} \xrightarrow{N_2H_4,\ OH^-} \text{N-doped graphene/}Fe_3O_4 + \text{Sulfosalicyclicacid ions}$$

Cite this: DOI: 10.1039/c0xx00000x

www.rsc.org/xxxxxx

ARTICLE TYPE

One-step synthesis of high-quality N-doped graphene/Fe_3O_4 hybrid nanocomposite and its improved supercapacitor performances

Li Li, Yuanyun Dou, Lifeng Wang, Min Luo and Jun Liang*

Received (in XXX, XXX) Xth XXXXXXXXX 20XX, Accepted Xth XXXXXXXXX 20XX

DOI: 10.1039/b000000x

A series of high-quality N-doped graphene (N-graphene)/Fe_3O_4 nanocomposites were readily obtained by a simple one-pot hydrothermal method under mild conditions. The as-prepared N-graphene/Fe_3O_4 hybrids were characterized by powder X-ray diffraction (XRD), fourier transform infrared spectroscopy (FT-IR), transmission electron microscopy (TEM), X-ray photoelectron spectroscopy (XPS), Raman spectroscopy, and thermogravimetric analysis (TGA). The experimental results demonstrated that ferromagnetic Fe_3O_4 nanocrystals (NCs) of sub-9 nm are facilely achieved and densely anchored onto the surface of N-graphene nanosheets. As an electrode material for electrochemical capacitors, the electochemical properties of N-graphene/Fe_3O_4 nanocomposites were tested, and it was interesting to find that the combination of N-graphene nanosheets with Fe_3O_4 NCs showed much higher specific capacitance than that of either pure N-graphene or pure Fe_3O_4 NCs, making them a promising electrode material for supercapacitors. Furthermore, the N-graphene hybrids also showed stable cycling performance along with 95% specific capacitance retained after 1000 cycle tests.

Introduction

Eletrochemical supercapacitors have been recognized as one type of promising energy storge devices owing to their unique properties and potential applications in areas of portable electrons, digital communication, hybrid electronic vehicles and renewable energy systems.[1] Recent investigations of the supercapacitors have demonstrated exceptional advantages such as high power delivery, high rates of charge/discharge, low maintenance cost, high cycle efficiency and almost unlimited cycle life.[2-4] However, one of the key challenges for eletrochemical capacitors is their limited energy density, which has hindered their wider application in the field of energy storage. To overcome this challenge, a major focus of supercapacitors research should be carried out to discover new hybrid electrode materials with high capacitance and a wide potential window.[5]

Owing to its new and/or enhanced functionalities that cannot be achieved by either component alone, Fe_3O_4-graphene composites have recently received increased attention for supercapacitor and Li ion battery applications.[6-9] Some successful examples are the development of reduced graphene oxide (rGO) sheets/iron oxide nanocomposites which have proven to be highly provided improved electrochemical performances due to their synergistic effects by combining the redox reaction of iron oxide and high surface area/conductivity of graphene. The rGO/Fe_3O_4 hybrid materials are usually achieved by *in situ* reduction of iron salt precursors and graphene oxide (GOs) as starting materials,[9,10] chemical precipitation method,[11-13] high-temperature decomposition of iron precursor,[14,15] assembly of the Fe_3O_4 NCs on the GO surface,[16] and deposition of Fe_3O_4 NCs on rGO sheets.[17] However, among these rGO sheets/iron oxide composites, it is a pity that only a limited number of experimental studies for N-graphene/Fe_3O_4 hybrids have been reported so far.[18, 19] Additionally, some theoretical or computational studies suggested that N-graphene could further expand its potential applications in supercapacitors field.[20,21] This is because the stronger electronegativity of nitrogen and conjugation between the nitrogen lone pair electrons and the graphene system can affect the supercapacitors performance.[20] Therefore, to exploit these potential applications, simple and scalable synthetic techniques for N-graphene/Fe_3O_4 hybrid materials are required.

In this paper, we report a novel and reliable approach to prepare highly qualified N-graphene/Fe_3O_4 nanocomposites via a simple hydrothermal process, which combines the *in situ* growth of the Fe_3O_4 NCs as well as simultaneous nitrogen doping and reduction of GOs in one single step in a aqueous solution of $[FeL_3]^{6-}$ (L, sulfosalicylic acid) and hydrated hydrazine. The structural features of N-graphene/Fe_3O_4 hybrids and its eletrochemical properties on the capacitive behavior are discussed. It is showed that the obtained nanocomposite indeed exhibit

* *College of Chemistry and Chemical Engineering, Ningxia University, Yinchuan 750021, PR China. ; Tel: +86 951 2062004*

E-mail: li_l@nxu.edu.cn; junliang@nxu.edu.cn.

† Electronic Supplementary Information (ESI) available: Table S1; Fig. S1-S2. See DOI:10.1039/b000000x/

significantly enhanced electrochemical specific capacitance and excellent electrochemical stability.

Experimental section

Materials and preparation: All reagents used in the experiment were of analytical grade and used without further purification. Graphene oxide (GO) was prepared from natural graphite powder (99%, Shanghai Sinopharm Chemical Reagent Co., Ltd.) using a modified Hummer's method.[22] A typical synthesis of the N-graphene/Fe_3O_4 hybrids was as follows: 0.08 g of GO was dispersed in deionized water and pretreated with ultrasonication for 2 h. 2 mmol of $FeCl_3 \cdot 7H_2O$ and 6 mmol of sulfosalicylic acid sodium were dissolved in 40 mL of deionized water under stirring, then 10 mL of N_2H_4 (80%) and appropriate amount of NaOH was added into the solution to form a stable complex solution (pH≈10.4). Finally, the suspension containing GO was slowly added into above complex solution, the whole mixture was stirred at room temperature for 12 h and transferred into a 100-mL Teflon-lined stainless steel autoclave, sealed, and maintained at 140℃ for 12 h. After the reaction completed, the black solid product was collected by centrifugation and washed several times with distilled water and anhydrous ethanol. The product was dried under vacuum at 60℃ for 12 h. The synthesis procedure of N-graphene was the same as N-graphene/Fe_3O_4 hybrids but without the addition of $FeCl_3$ in the first step. Bare Fe_3O_4 was obtained through the same steps as N-graphene/Fe_3O_4 without adding GO in the second step.

Physicochemical Characterization

The phase purity and crystal structure of the sample were characterized by powder X-ray diffraction (XRD) on a D/Max 2200V/PC X-ray diffractometer with Cu Kα radiation (λ=1.54187 Å). More details about the chemical structure and morphology of the sample were obtained from selected-area electron diffraction (SAED) combined with high-resolution transmission electron microscopy studies (HRTEM, FEI Tecnai F30 transmission electron microscope). X-ray photoelectron spectroscopy data were obtained with an ESCALab220i-XL electron spectrometer from VG Scientific using 300W AlKα radiation. The base pressure was about 3×10^{-9} mbar. The binding energies were referenced to the C1s line at 284.8 eV from adventitious carbon. Raman spectroscopic measurements were performed on a Renishaw inVia Raman System 1000 with a 532 nm Nd:YAG excitation source at room temperature. The insight chemical characterization of the samples was analyzed by FT-IR (FTIR-8400S). The magnetic property of the sample was measured by a BHV-55 vibrating sample magnetometer at room temperature. The composition of N-graphene/Fe_3O_4 nanocomposites were determined by the thermal gravimetric analysis using a TA Instruments Q500 Thermogravimetric Analyzer (TGA) with a heating rate of 5/℃ min^{-1} under dry air.

Electrochemical testing

The electrochemical properties and capacitance measurements of the supercapacitor electrodes were studied in a three-electrode system in 1 M sulfuric acid electrolyte, whereas, a platinum foil electrode as the counter electrode, and an Ag/AgCl electrode as the reference electrode (RE). To fabricate working electrodes (WE) for supercapacitors, 80 wt% the N-graphene/Fe_3O_4 (Fe_3O_4 NCs or N-graphene) active materials, 10 wt% carbon black and 10 wt% polyvinlidene fluoride (PVdF) binder were mixed together and ground thoroughly. Ethanol was added to the mixture to form a slurry, which was pasted on graphite plate. The electrodes pretreated by Nafion solution were dried under vacuum at room temperature for 12 h. Cyclic voltammetry (CV) measurements were conducted from -0.2 to 0.8 V vs. Ag/AgCl at 10, 20, 50 and 100 mV s^{-1} on an electrochemistry workstation (CHI660D). The galvanostatic charge–discharge characteristics were examined by a chronoamperometry technique on the same electrochemistry workstation. The voltage range was set to -0.2-0.8 V with current rates of 1 A g^{-1} and 8 A g^{-1} for 1000 cycles. Electrochemical impedance spectroscopy (EIS) measurements were carried out in the frequency range from 10^6 Hz to 0.01 Hz at open circuit potential with an ac perturbation of 5 mV. The specific capacitance C_m of N-graphene/Fe_3O_4 electrode film from CV can be calculated by the equation (1):

$$C_m = \frac{1}{m \cdot s \cdot \Delta V}\int_{V1}^{V2} IdV \qquad (1)$$

where m is the mass of N-graphene/Fe_3O_4, ΔV is the potential window, s is the scan rate, here s=10 mV s^{-1}, I is the instaneous charge current in given potential. In addition, the specific capacitance can be calculated from the galvanostatic charging-discharging function according to the equation 2:

$$C_m = \frac{I\Delta t}{\Delta V m} \qquad (2)$$

In this equation, C is the specific capacitance, I is the current, Δt is the discharging time, ΔV is the potential window, and m is mass of the electroactive material.

Results and discussion

Scheme 1 shows the schematic procedure for preparation of the N-graphene/Fe_3O_4 material. In our cases, it is important to note that hydrated hydrazine can serve as both a reducing reagent and a doping agent for the formation of N-graphene/Fe_3O_4 hybrids in present synthetic system. The possible process mechanism is suggested as follows:

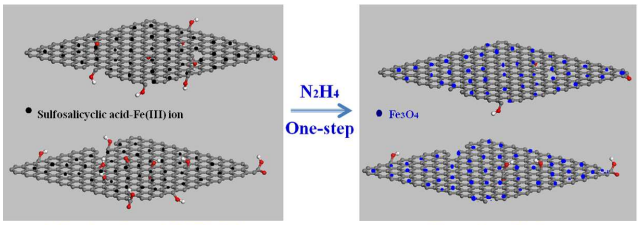

$$\left[Fe^{III}(\text{sulfosalicylic acid})_3\right]^{6-} + \text{Graphene oxide} \xrightarrow{N_2H_4,\ OH^-} \text{N-doped graphene/}Fe_3O_4 + \text{Sulfosalicylicacid ions}$$

Scheme 1 Schematic diagram of the synthesis of N-graphene/Fe_3O_4 nanocomposite.

First, under OH^- synergistic effects (pH≈10.4), sulfosalicylic acid ions (L) can coordinate with Fe^{3+} to form a $[FeL_3]^{6-}$ complex ion. These complex ions can be densely absorbed on the surface of GO nanosheets (Scheme 1). Then, $[FeL_3]^{6-}$ ion dissociated slowly into Fe(III) ions under the present hydrothermal

conditions. Fe(III) can be reduced into Fe(II) by N_2H_4 in alkalescence medium. Consequently, Fe_3O_4 is formed by the reaction between Fe(III) and Fe(II) in alkalescence solution.[26] Meanwhile, these Fe_3O_4 NCs are monodispersedly in-situ anchored onto the surface of N-graphene nanosheets (Scheme 1). Additionally, regarding to the formation of N-graphene, preparation of N-graphene sheets by a combined chemical and hydrothermal reduction of graphene oxide using N_2H_4 and/or NH_3 has been reported by Long et al, [21] and they believed that these nitrogen atoms should inherit from the reducing reagent N_2H_4 and/or ammonia. In view of reasons reported above, N-graphene/Fe_3O_4 composites are naturally obtained by present one-step hydrothermal process.

X-ray powder diffraction (XRD) is employed to determine the crystallographic phases of the products. A strong (002) diffraction peak is observed at 10.5° in Fig. 1A(a), indicating that GO has been obtained by the chemical oxidation of graphite powder. The phase purity of the as-prepared N-graphene/Fe_3O_4 nanocomposite is also confirmed in Fig 1A(c). As for N-graphene/Fe_3O_4 sample, the very broad peak at 25~26° can be attributed to those of N-graphene (Fig 1A(b)) and the complete disappearance of the peak at 10.5° shows that the reduction of GO is completed in present hydrothermal reduction process. Additionally, the peaks located at 2θ =18.27, 30.1, 35.42, 43.05, 53.4, 56.95, and 62.52° in Fig 1 A(c) were assigned to the (111), (220), (311), (222), (400), (422), (511), and (440) reflections of the Fe_3O_4, respectively, and all the diffraction peaks can be indexed to a pure face-centered cubic phase (fcc, space group Fd-3m) of Fe_3O_4 (JCPDS card no.19-0629). XRD analysis suggests that the hybrid material is composed of Fe_3O_4 and graphene.

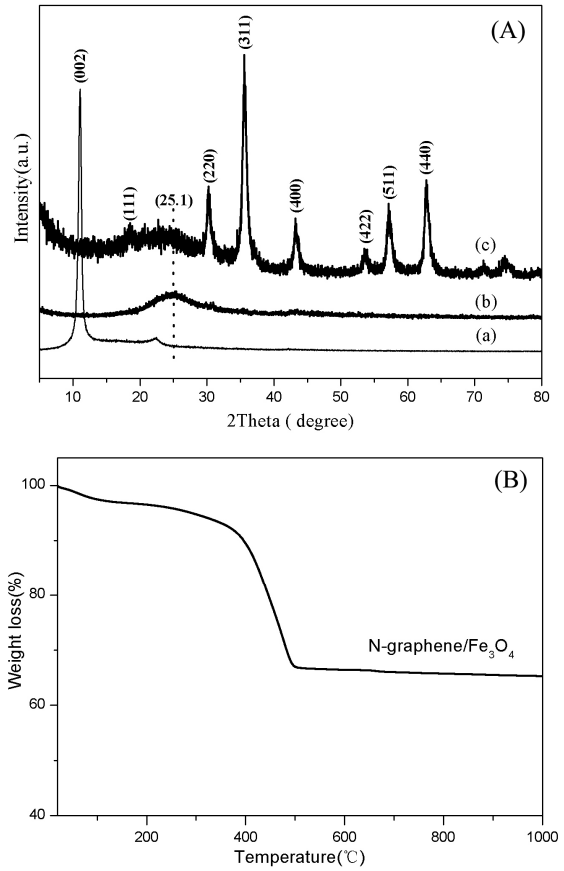

Fig. 1 (A) Typical powder XRD patterns of the as-obtained (a) GO, (b) N-graphene, and (c) N-graphene/Fe_3O_4 nanocomposite. (B) TGA curve of N-graphene/Fe_3O_4 in air ranging from 20 ℃ to 1000 ℃.

The content of Fe_3O_4 in N-graphene/Fe_3O_4 hybrids was determined by thermogravimetric analysis (TGA). Fig. 1B shows the TGA graph of the N-graphene/Fe_3O_4 nanocomposite. The TGA measurement identified the weight losses of N-graphene/Fe_3O_4 from 20 ℃ to 1000 ℃ in air. There are several stages of weight loss for N-graphene/Fe_3O_4, which could be ascribed to different phase changes in the air atmosphere. However, the weight loss from 400 ℃ to 640 ℃ is due to the burning of N-graphene in air. Therefore, it can be determined that the weight composition of the N-graphene/Fe_3O_4 nanocomposite is about 36wt% graphene and 64 wt% Fe_3O_4.

Fig. 2 displays typical FT-IR spectra of GO and N-graphene/Fe_3O_4 nanocomposite. The characteristic of peaks of GO, including O-H (v_{O-H} at 3400 cm^{-1}), C=O ($v_{C=O}$ at 1725 cm^{-1}), skeletal vibration of unoxidized graphitic domains at 1620 cm^{-1}, OH ($v_{O=H}$ at 1412 cm^{-1}), C-OH (v_{C-OH} at 1220 cm^{-1}), and C-O (v_{C-O} at 1061 cm^{-1}), were clearly observed in the FT-IR spectrumof GO (Fig. 2a).[23] However, for the N-graphene/Fe_3O_4 sample (Fig. 2b), all these absorption peaks related to oxidized groups decreased dramatically in the FT-IR spectrum of N-graphene/Fe_3O_4 nanocomposite prepared from GO, suggesting the reduction of above-mentioned functional groups by hydrazine hydrate, while a new absorption band that appears at about 1571 cm^{-1} corresponds to the aromatic skeletal C=C stretching vibration of the reduced graphene oxide sheets,[23] In addition, N-graphene/Fe_3O_4 composite (Fig. 2b) presents one band at 581 cm^{-1} that is characteristic of stretching vibration of Fe-O band for Fe_3O_4.[24] These results demonstrates the coexistence of graphene and Fe_3O_4 species under present hydrothermal system.

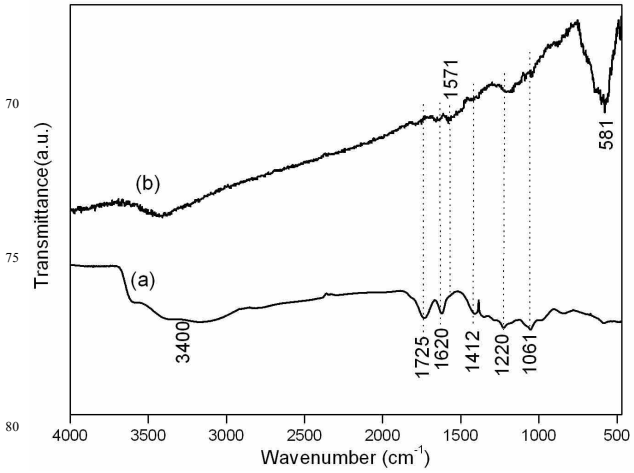

Fig. 2 Typical FT-IR spectra of GO (a) and N-graphene/Fe_3O_4 nanocomposite (b).

The products obtained were further examined by X-ray photoelectron spectroscopy (XPS). The fully scanned spectra demonstrated that C and O elements existed in GO sample (Fig.

3a), whereas after hydrothermal reaction in the presence of $[FeL_3]^{6-}$, hydrated hydrazine and GO, the XPS spectrum indicated the presence of N, Fe elements in the composites, besides C and O (Fig 3b). Inset in parts (a) and (b), the deconvoluted XPS peaks of C1s centered at the binding energies of 289.3, 287.5, 286.3, and 284.7 eV were assigned to the C(O)O, C=O, C-O, and C-C, respectively.[16, 25] It can be clearly seen that most carbon atoms were sp^2 hybridized, and the intensity of oxygenated functional groups (HO-C=O, C-O-C, and C-OH) on carbon sheets in N-graphene/Fe_3O_4 was obviously decreased compared with that of GO, while the C–N groups at ca. 285.7 eV (Fig 3b) suggest that nitrogen atoms were introduced into the graphene nanosheets during the reduction, which came from the reducing agent N_2H_4. The high-resolution N 1s scan (Fig. 3d) further showed the presence of one form of pyridinic N (398.1 ± 0.2eV).[18] This indicates that GO could be reduced to N-graphene with a tiny amount of residual oxygen-containing groups via hydrothermal reaction. Upon hydrothermal reduction, the nitrogen content in the graphene is ca. 2.1% by elemental analysis, some study believed that these nitrogen atoms doped in the graphene sheets should come from the reducing reagent N_2H_4 and/or ammonia during the hydrothermal reaction.[21] Furthermore, the spectra of the sample corresponding to the binding energies of Fe 2 p are shown in Fig. 3c . It shows that the photoelectron peaks of 711.1, 724.5 correspond to $Fe2p_{2/3}$ and $Fe2p_{1/2}$, respectively.The data are consistent with the values in the literature,[26] which further proves the composition of the magnetic Fe_3O_4. The XPS result is in good agreement with the Fourier transformed infrared spectroscopy (FT-IR).

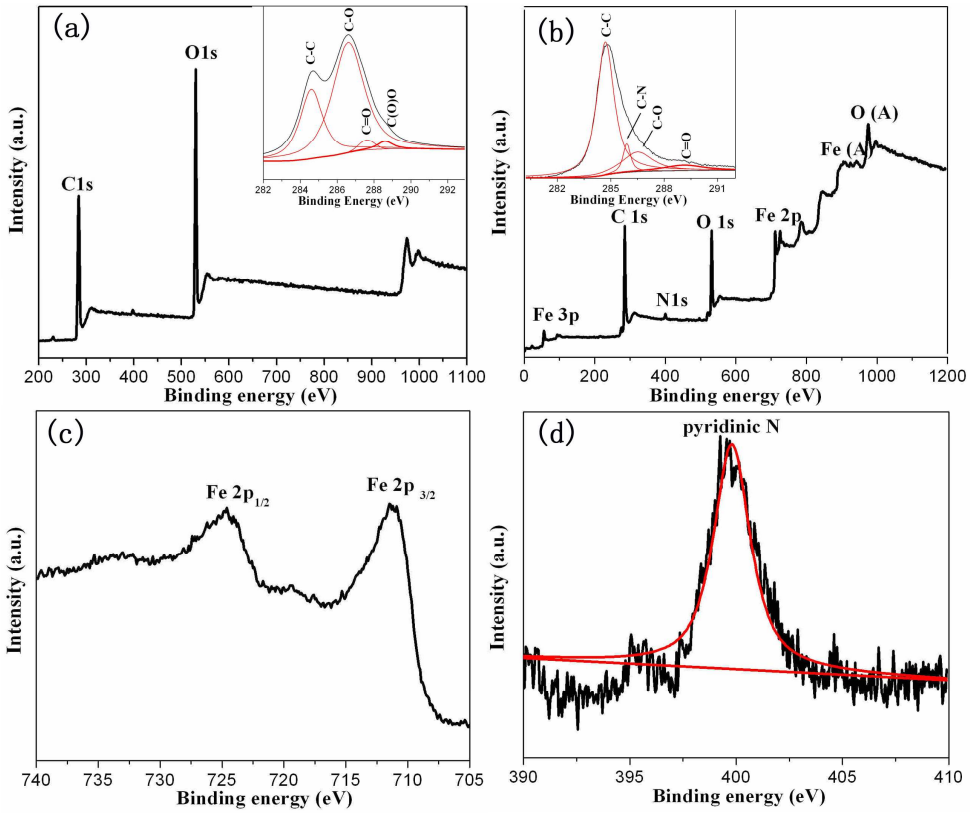

Fig. 3 XPS spectra of GO and N-graphene/Fe_3O_4. (a) GO; (b) N-graphene/Fe_3O_4; (c) Fe 2p spectrum of N-graphene/Fe_3O_4; (d) N1s of N-graphene/Fe_3O_4. Inset in parts (a) and (b): the corresponding high-resolution spectra of C1s, respectively.

Raman spectroscopy is a powerful tool for identifying carbon materials and detecting the doping effect of graphene. We ought to pay attention to is that the intensity ratio of the D band (~1348 cm^{-1}) and G band (~1586 cm^{-1}), I_D/I_G, is a measure of the relative concentration of local defects or disorders (particularly the sp^3-hybridized defects) compared to the sp^2-hybridized N-graphene domains. It can be seen from Fig. 4A that the I_D/I_G ratio is 0.97 for GO. After the hydrothermal reaction, the I_D/I_G ratio is increased to 1.05, thus indicating the improvement of the disordered N-graphene sheets in N-graphene/Fe_3O_4 nanocomposite resulting from the hydrothermal reduction process.[27] The high intensity of the D-band in the N-graphene sheets clearly implies the presence of defects in the N-graphene layer; these defects are usually generated during nitrogen doping. In addition, as compared to Raman spectra of graphite, we can confirm that it is N-graphene rather than graphite in the hybrid nanocomposites. To verify the number of N-graphene layers in the produced nanocomposites, we have analyzed the variation of the 2D band at ~ 2696 cm^{-1}, as displayed in Fig. 4B. The 2D peaks of the N-graphene/Fe_3O_4 nanocomposite and N-graphene

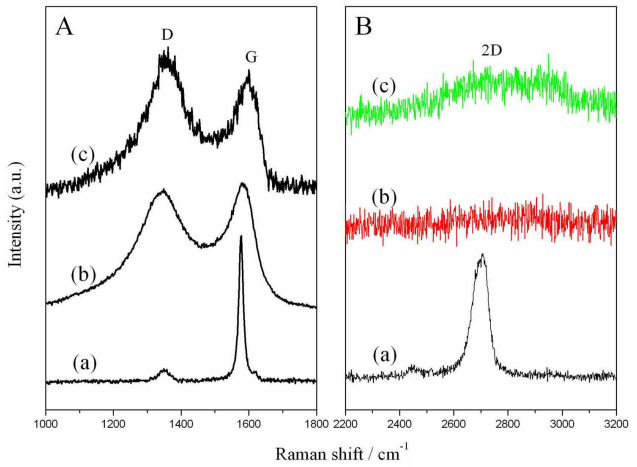

Fig. 4 (A) Raman spectra of graphite (a), GO (b) and N-graphene/Fe_3O_4 nanocomposite (c) at room temperature. (B) Raman spectra of graphite (a), N-graphene (b) and N-graphene/Fe_3O_4 nanocomposite (c) at room temperature.

are found with lower intensity than graphite powders, indicating the restack and agglomeration of N-graphene sheets occur in the reduction of GO to N-graphene. In addition, it can be referred from the intensity and location of 2D peak for N-graphene/Fe_3O_4 that the number of N-graphene layers in the nanocomposite is not single or bistratal but multilayer.[28]

The morphology and structure of the as-obtained N-graphene/Fe_3O_4 nanocomposite were investigated by means of TEM. The low-magnification TEM image (Fig. 5a) shows a crumpled sheet-like morphology with about several micrometers in diameter. In generally, the morphology of graphene was attributed to defective structures formed upon exfoliation or the presence of doped nitrogen atoms. The similar effects of nitrogen doping can be observed in previous work.[29] A large amount of Fe_3O_4 NCs dispersed on layered N-graphene substrate was

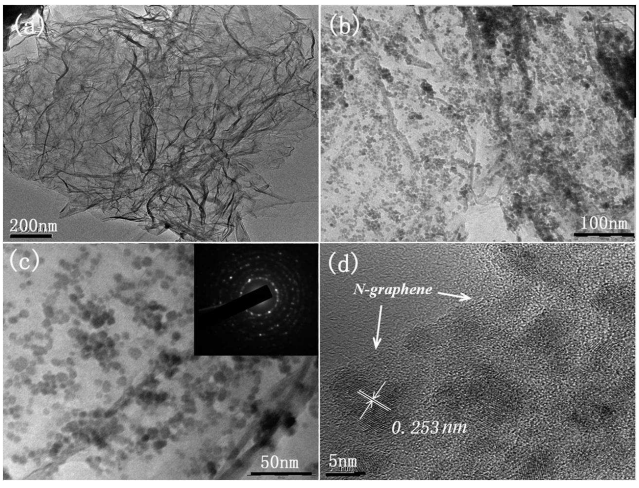

Fig. 5 (a) Typical TEM image of the as-obtained N-graphene. Typical low-magnification (b) and high-magnification (c) TEM images of the N-graphene/Fe_3O_4 hybrids obtained. (d) HRTEM image of N-graphene/Fe_3O_4 nanocomposite. Inset in panel (c) is the corresponding SAED pattern of Fe_3O_4 in N-graphene/Fe_3O_4 sample.

detected, as shown on a typical TEM image in Fig. 5b. The as-prepared ferromagnetic Fe_3O_4 NCs are monodispersedly anchored onto the N-graphene nanosheets. Fig. 5c shows a partially enlarged TEM image of the as-prepared product. It can be clearly observed that the size of Fe_3O_4 NCs on N-graphene is in the range of 5–9 nm, and clearly the layered N-graphene is covered with Fe_3O_4 on its surface. TEM images indicate that monodispersed Fe_3O_4 NCs can be facilely synthesized on the N-graphene sheets by one-step hydrothermal process. In addition, to further obtain the detailed crystal structure of Fe_3O_4 NCs in N-graphene/Fe_3O_4 hybrid, the high-resolution transmission electron microscopy (HRTEM) observations were carried out. Fig. 5d shows typical HRTEM image of the graphene hybrids, according to the image, well-resolved lattice fringes are clearly visible across entire nanocrystals, with an interplanar distance of 0.253 nm corresponding to the (311) d spacing of the cubic Fe_3O_4 structure. The selected area electron diffraction (SAED) (insert in Fig. 5c) verifies that the Fe_3O_4 NCs in N-graphene/Fe_3O_4 sample show apparently single crystalline characteristic.

To explore its potential applications in energy storage, N-graphene/Fe_3O_4 nanocomposite was fabricated into supercapacitor electrode and characterized using cyclic voltammetry (CV) and galvanostatic charge-discharge measurements. For the comparison, electrochemical properties of the Fe_3O_4 NCs and N-graphene were also determined. Fig. 6a shows representative CV curves of the Fe_3O_4 NCs, N-graphene and N-graphene/Fe_3O_4 nanocomposite at a scan rate of 10 mV s^{-1}. Among these profiles, the CV curve of the N-graphene had a rectangular shape within a potential window of -0.2 to 0.8 V which was characteristic of double-layer capacitance. However, the CV curves of Fe_3O_4 NCs and N-graphene/Fe_3O_4 hybrids are nearly symmetrical with redox peaks. It is evident that the samples demonstrate pseudo-capacitive properties. The redox peaks appear in the CV curves are assumed to represent the reduction/oxidation of Fe(II) and Fe(III). It is important to note that the current and area in the CV curve for N-graphene/Fe_3O_4 sample is apparently much higher than those of N-graphene and Fe_3O_4 NCs at the same scan rate. The result indicates that N-graphene/Fe_3O_4 hybrids have the highest specific capacitance. On the contrary, Fe_3O_4 NCs show the lowest specific capacitance compared to N-graphene and N-graphene/Fe_3O_4 nanocomposite. The calculated specific capacitance is 220 F g^{-1} for N-graphene/Fe_3O_4 nanocomposite at a scan rate of 10 mV $\mathbf{s^{-1}}$ (Fig. 6a), which is much higher than that of pure Fe_3O_4 (i.e. 55 F g^{-1}) and N-graphene (i.e. 106 F g^{-1}) electrodes.

Galvanostatic charge-discharge behaviors of these samples were also performed at the specific current of 1 A g^{-1} in the potential range between -0.2 and 0.8 V (Fig. 6b). It can be seen that all these materials showed highly reversible charge-discharge profiles during the electrochemical processes. For N-graphene/Fe_3O_4 hybrid, the nonlinear feature of the curve confirms that the charge-discharge processes primarily arise from the surface Faradaic redox reaction, but are not dominated by the electrochemical double-layer capacitance. Nonetheless, it should be noted that the N-graphene/Fe_3O_4 electrode undertook much longer charge-discharge process than those of the pure N-graphene and Fe_3O_4 NCs electrodes. This indicated a much higher electric storage capacity of the N-graphene/Fe_3O_4

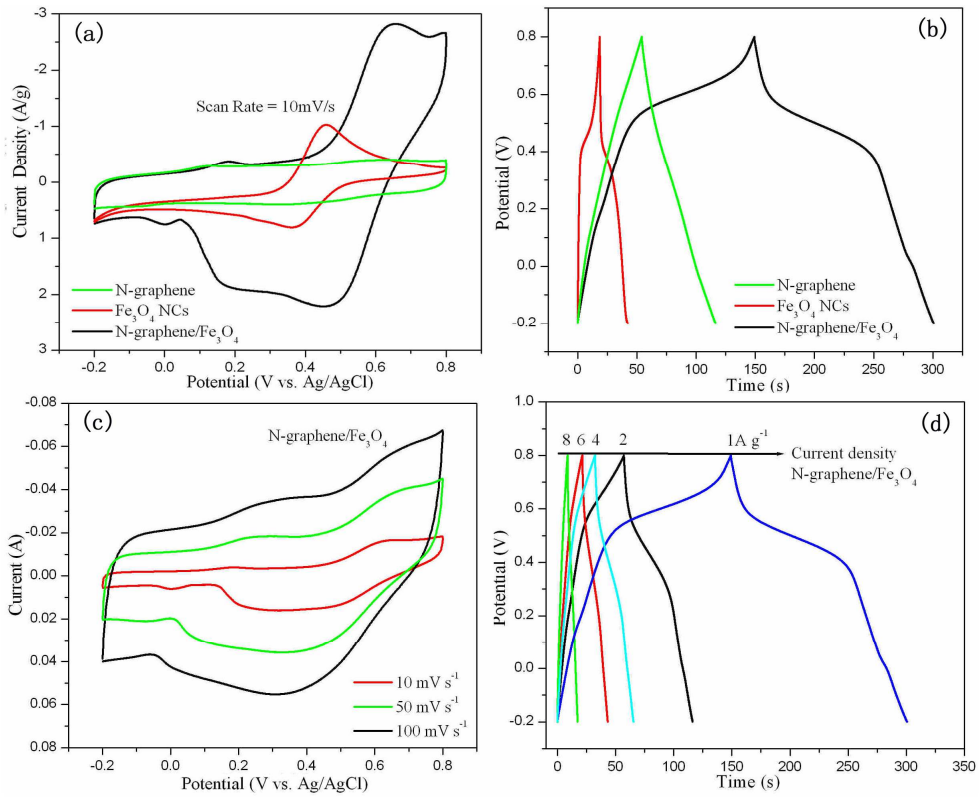

Fig. 6 (a) Cyclic voltammetry curves of the Fe_3O_4 NCs, N-graphene and N-graphene/Fe_3O_4 nanocomposite at a scan rate of 10 mV s^{-1}. (b) Galvanostatic charge-discharge curves of Fe_3O_4 NCs, N-graphene and N-graphene/Fe_3O_4 nanocomposite electrode at a current density of 1 A g^{-1}. (c,d) Cyclic voltammetry and galvanostatic charge-discharge curves of the N-graphene/Fe_3O_4 nanocomposite electrode at different scan rates and current desities

electrode. The significant enhancement in specific capacitance can be a positive synergistic effect that the homogeneous dispersion of N-graphene sheets superimposes on pseudocapacitance from Fe_3O_4 on double-layer capacitance from N-graphene.

Fig. 6c shows the typical CV curves of the N-graphene/Fe_3O_4 hybrids at different scan rates. Very clearly, the peak current increases with insignificant change in the CV shape when scan rates increase from 10 to 100 mV s^{-1}, which reveals its good electrochemical reversibility and high power characteristics. The largest specific capacitance of 220 F g^{-1} can be reached at a scan rate of 10 mV s^{-1}, which is nearly consistent with the largest value (212 F g^{-1}, at 1A g^{-1}) calculated from the charge-discharge curve (Fig. 6d). In addition, when the current density is increased from 1 A g^{-1} to 8 A g^{-1}, the specific capacitance can still remain at a high level above 172 F g^{-1} with a good retention of about 82% (Fig. 6d). These results indicate that the integration of N-graphene material and Fe_3O_4 NCs greatly boosts the energy storage performance.

The enhanced electrochemical performance of the N-graphene/Fe_3O_4 nanocomposite was further confirmed by the electrochemical impedance spectroscopy (EIS) measurements. Fig. 7 presents the Nyquist plots of supercapacitors made of Fe_3O_4 NCs, N-graphene and N-graphene/Fe_3O_4 electrodes in the frequency range from 10^6 to 10^{-2} Hz. According to analysis of Nyquist plots, the N-graphene/Fe_3O_4 hybrid exhibits the lowest charge-transfer resistance and thus allow for an excellent conductivity. The ideal capacitor always exhibits a vertical line at low frequency. As shown in Fig. 7, the plot of the N-graphene/Fe_3O_4 supercapacitor starts with a ca. 80° impedance line and approaches an almost vertical line at low frequency.

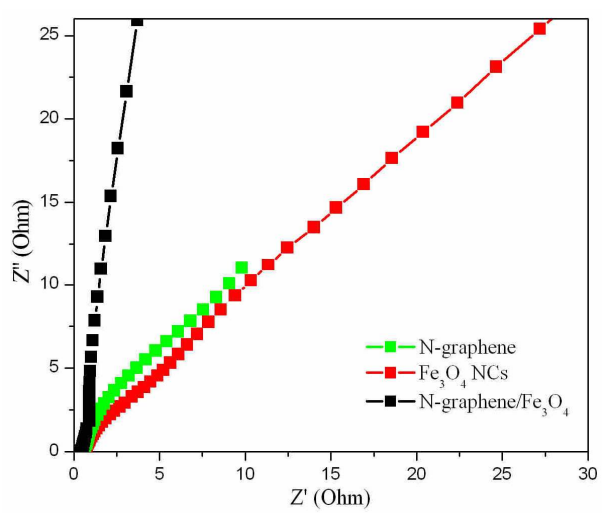

Fig. 7 The Nyquist impedance plots of N-graphene, Fe_3O_4 NCs and N-graphene/Fe_3O_4 nanocomposite.

Long cycle life of supercapacitors is a key factor to evaluate the electrodes for their practical applications. In order to further examine the cycle perfomances of the as-obtained samples, cyclic voltammetry (CV) measurements were conducted from -0.2 to 0.8 V vs . Ag/AgCl electrode at 10 mV s^{-1} of the pure Fe_3O_4, N-graphene and N-graphene/Fe_3O_4 nanocomposite were shown in Fig. 8. As can be seen, the N-graphene/Fe_3O_4 nanocomposite shows the highest specific capacitance during cyclic voltammetry for 1000 cycles, and the specific capacitance value is decreased in the order N-graphene/Fe_3O_4 > N-graphene > Fe_3O_4 NCs. More importantly, It can be observed from Fig. 8 that the specific capacitance retention of as-obtained N-graphene/Fe_3O_4 nanocomposite was over 95% after 1000 cycle tests, indicating its excellent electrochemical stability and cycling performance. However, there was about 35% decay for the pure Fe_3O_4 NCs in the available capacity over 1000 cycles.

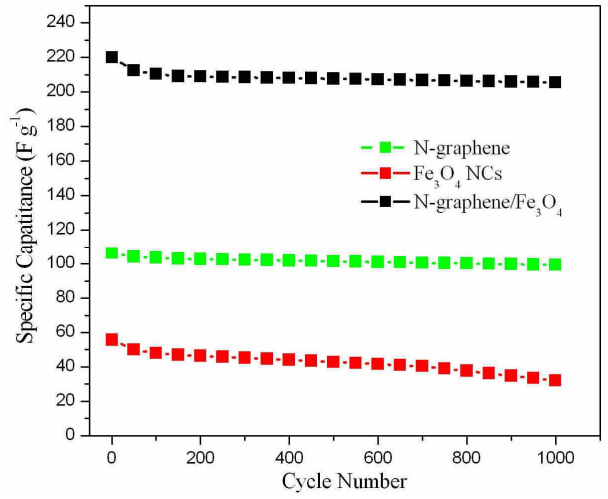

Fig. 8 Cycle life of N-graphene, Fe_3O_4 NCs and N-graphene/Fe_3O_4 nanocomposite at 10 mV s^{-1}.

Based on the preceding structural characterizations and above electrochemical properties and capacitance measurements, in our cases, the high specific capacitance and good cycle performance delivered by N-graphene/Fe_3O_4 electrode may be mainly ascribed to the following three factors. First, some studies[1,3] have demonstrated that graphene-based nanohybrids not only facilitated electronic and ionic conduction due to the presence of highly conductive graphene and well-directed conductive paths, but also avoided the loss of cyclability during repetitive incorporation/extraction processes due to the flexible graphene, which would feasibly buffer the mechanical stress. Second, in our cases, the high-quality N-graphene/Fe_3O_4 nanocomposites can not only alleviate the aggregation of Fe_3O_4 NCs and N-graphene nanosheets to improve the connection between active materials and electrolyte, but also provide an excellent electrical conductivity in the overall electrode. Additionally, combining different materials to form composites should be an important approach because the individual substances in the composites can have a synergistic effect through minimizing particle size, enhancing chemical corrosion resistant, preventing particles from agglomerating, protecting active materials from mechanical degradation. Herein, on the basis of the electrochemical results analysis reported above, we believed that the significant enhancement in electrochemical performance over N-graphene/Fe_3O_4 nanocomposite should be attributed to a positive synergetic effect that the homogeneous dispersion of N-graphene sheets superimposes on pseudocapacitance from Fe_3O_4 on double-layer capacitance from N-graphene nanosheets. As a result, the as-obtained N-graphene/Fe_3O_4 nanocomposites can overcome the drawbacks of the individual substances and embody the advantages of all constituents.

Conclusions

In this work, an N-graphene/Fe_3O_4 nanocomposite was prepared by a facile and reliable one-step hydrothermal method, in which sub-9 nm Fe_3O_4 NCs were densely dispersed between N-graphene nanosheets. The as-prepared nanocomposite showed significantly enhanced electrochemical specific capacitances, which reached 220 F g^{-1} at a current rate of 10 mV s^{-1}. The N-graphene/Fe_3O_4 nanocomposite also demonstrated excellent cycling stabilities. In comparison with bare N-graphene sheets and Fe_3O_4 NCs, the overall electrochemical performance of the N-graphene/Fe_3O_4 nanocomposite has been drastically improved. The significant enhancement in specific capacitance and cycle performance can be a result of the synergistic effect by combining the redox reaction of Fe_3O_4 NCs and high surface area/conductivity of N-graphene. Furthermore, the superior electrochemical properties of the N-graphene/Fe_3O_4 nanocomposite may lead to potential applications for high-performance supercapacitors.

Acknowledgement

This work was supported by the National Natural Science Foundation of China (Grant No. 21361019 and 21361020), and the Natural Science Foundation of Ningxia Province (Grant No. NZ 1104).

References

1 G.P. Wang, L. Zhang and J.J. Zhang , *Chem. Soc. Rev.* 2012, **41**, 797.
2 D. Qu, *J. Power Sources*, 2002, **109**, 403.
3 M. Winter and R.J. Brodd, *Chem. Rev.*, 2004, **104**, 4245.
4 D. Choi, G.E. Blomgren and P.N. Kumta, *Adv. Mater.*, 2006, **18**, 1178.
5 Y.B. Tan and J.–M. Lee, *J. Mater. Chem. A*, 2013,**1**, 14814.
6 B.J. Li, H.Q. Cao, J. Shao and M.Z. Qu, *Chem. Commun.*, 2011, **47**, 10374.
7 X.Y. Li, X.L. Huang, D.P. Liu, X. Wang, S.Y. Song, L. Zhou and H.J. Zhang, J. Phys. Chem. C, 2011, **115**, 21567.
8 J. Su, M.H. Cao, L. Ren and C.W. Hu, *J. Phys. Chem. C*, 2011, **115**, 14469.
9 G.M. Zhou, D.W. Wang, F. Li, L. Zhang, N. Li, Z.S. Wu, L. Wen, G.Q. Lu and H.M. Cheng, *Chem. Mater.*, 2010, **22**, 5306.
10 Y. H. Xue, H. Chen, D.S. Yu, S.Y. Wang, M. Yardeni, Q.B. Dai, M. Guo, Y. Liu, F. Lu and J. Qu, *Chem. Commun.*, 2011, **47**, 11689.
11 X.Y. Yang, X.Y. Zhang, Y.F. Ma, Y. Huang, Y.S. Wang and Y.S. Chen, *J. Mater. Chem.*, 2009, **19**, 2710.
12 V. Chandra, J. Park, Y. Chun, J. Woo Lee, In-C. Hwang and K. S. Kim, *ACS Nano*, 2010, **4**, 3979.
13 Shantanu K. Behera, *Chem. Commun.*, 2011, **47**, 10371.
14 Y.J. Gao, D. Ma, G. Hu, P.Z., X.H. Bao, B. Zhu, B. Zhang and D.S. Su, *Angew. Chem. Int. Ed.*, 2011, **50**, 1.
15 Y. Zhang, B. Chen, L. Zhang, J. Huang, F.H. Chen, Z.P. Yang, J.L. Yao and Z.J. Zhang, *Nanoscale*, 2011, **3**, 1446.

16 F. He, J. T. Fan, D. Ma, L. M. Zhang, C. Leung and H.L. Chan, *Carbon*, 2010, **48**, 3139.
17 S.M. Zhu, J.J. Guo, J.P. Dong, Z.W. Cui, T. Lu, C.L. Zhu, D. Zhang and J. Ma, Ultrason. Sonochem., 2012, **8**, 6411.
18 Z.S. Wu, S.B. Yang, Y. Sun, K. Parvez, X.L. Feng, and K. Müllen, *J. Am. Chem. Soc.* 2012, **134**, 9082.
19 Y.H. Chang, J. Li, B. Wang, H. Luo, H.Y. He, Q. Song and L.J. Zhi, *J. Mater. Chem. A***,** 2013, **1**, 14658.
20 X.L. Li, H.L. Wang, J.T. Robinson, H. Sanchez, G. Diankov and H.J. Dai, *J. Am. Chem. Soc.*, 2009, **131**, 15939.
21 D.H. Long, W. Li, L.C. Ling, J. Miyawaki, I. Mochida and S.-H.H. Yoon, *Langmuir*, 2010, **26**, 16096.
22 W.S. Hummers, R.E. Offeman, *J. Am. Chem. Soc.*,1958, **80**,1339.
23 J.F. Shen, B. Yan, M. Shi, H.W. Ma, N. Li and M.X. Ye, *J. Mater. Chem.*, 2011, **21**, 3415.
24 J. Liang, L. Li, M. Luo, J.Z. Fang and Y.R. Hu, *Solid State Sci.*, 2010, **12**,1422.
25 B.J. Jiang, C.G. Tian, L. Wang, L. Sun, C. Chen, X.Z. Nong, Y.J. Qiao and H.G. Fu, *Appl. Surf. Sci.*, 2012, **258**, 3438.
26 J. Liang, L. Li, M. Luo, J.Z. Fang and Y.R. Hu, *Solid State Sci.*, 2010, **12**,1422.
27 A. C. Ferrari and J. Robertson, *Phys Rev B*, 2000, **61**, 14095.
28 C. Zhang, S.Q. Liu, M.-Q. Yang and Y.-J. Xu, *ACS Appl. Mater. Interfaces*, 2013, **5**, 4309.
29 L.S. Panchakarla, K.S. Subrahmanyam, S.K. Saha, A. Govindaraj, H.R. Krishna-murthy, U.V. Waghmare and C.N.R. Rao, *Adv. Mater.*, 2009, **21**, 4726.